Toward obtaining the propulsive factors for a wind-assisted ship

Downloaded from: https://research.chalmers.se, 2026-11-07 11:21 UTC

Citation for the original published paper (version of record):
Bakari, A., Alves Lopes, R., Eslamdoost, A. et al (2025). Toward obtaining the propulsive factors for a wind-assisted ship. [Source Title missing]: 14-20

N.B. When citing this work, cite the original published paper.

research.chalmers.se offers the possibility of retrieving research publications produced at Chalmers University of Technology. It covers all kind of research output: articles, dissertations, conference papers, reports etc. since 2004. research.chalmers.se is administrated and maintained by Chalmers Library

(article starts on next page)

Toward obtaining the propulsive factors for a wind-assisted ship

Abdoul-Malik BAKARI[1*], Rickard Bensow[1], Rui Lopes[2], and Arash Eslamdoost [1]
[*]Chalmers University of Technology, 41296, Gothenburg, Sweden
bakari@chalmers.se

1 Introduction

Wind sails for ship propulsion offer a promising alternative for reducing fuel consumption. The potential impact of the power produced by sails can reduce the fuel consumption from 10% to 30% according to a recent study (Ammar and and Seddiek, 2022; Ouchi et al., 2013). To enhance power prediction for wind-assisted vessels, it is crucial to develop a comprehensive understanding of how wind sails impact the hydrodynamics of the vessel, beside the aerodynamics. Numerical methods based on Computational Fluid Dynamics (CFD) are increasingly being adopted for ship power prediction and have become valuable tools in evaluating the power of Wind-Assisted Ship Propulsion (WASP).

When a ship operates with sails, the hull is subjected to aerodynamic side forces, resulting in a leeway and heel angle relative to the direction of motion (Clayton, 1987). Leeway angles, which are considered equivalent to the drift angle in the context of this study, will affect the hydrodynamic forces of the ship. The objective of this work is to evaluate the influence of drift angle on the hydrodynamic performance of a bare hull, with a specific focus on resistance components and analysis of the wake. CFD simulations are employed to determine the forces acting on the hull, the wake and the trained Proper Orthogonal Decomposition (POD) with Radial Basis Function (RBF) (Huayamave et al., 2017) interpolation network is utilised to efficiently predict wake fields, bypassing the need for additional CFD simulations. A thorough understanding of these effects is a step toward mapping the propulsive factors for WASP and crucial for effective integration of wind propulsion into ship design and operation.

2 Methods and setup

The test case used in this study is Jores1 tanker, a single screw tanker vessel. The main particulars of the ship are presented in Table 1. The study is divided into two main parts. The first part involves a double-body simulations of the hull using Reynolds-Averaged Navier-Stokes (RANS) equations at various drift angles (0° to 9°). This analysis aims to quantify the effects of drift angle on resistance components, including frictional resistance (RF), pressure resistance (RP), and viscous resistance (RV). Since wave resistance is neglected in this double-body framework, the total resistance (RT) is equated to viscous resistance (RT = RV = RF + RP). Additionally, the study evaluates the side force acting on the hull and the associated change in wake field induced by variations in the drift angle. The second part involves wake field prediction based on the POD-RBF method, utilising data from the CFD simulations to generate wake fields for various drift angles.

Table 1: Jores1tanker hull main particulars.

Parameter	Full scale	Model scale
Length between perpendiculars Lpp (m)	178.50	6.86
Breadth (m)	32.26	1.24
Draught at fore perpendicular (m)	10.56	0.406
Draught at aft perpendicular (m)	10.38	0.399
Draught at midship (m)	10.47	0.402
Wetted surface area (m^2)	8337.10	12.68
Displaced volume (m^3)	46648	2.86

CFD simulations were conducted for both full-scale and model-scale vessels. The numerical simulation was performed using Simcenter STAR-CCM+ (version 2024.10.1) software. The transport equations are solved using the finite volume method. A segregated solver utilizing the SIMPLE algorithm is employed for pressure-velocity coupling. All simulations assumed to be steady-state. A geometric scale ratio of 1/26 was applied for model-scale simulations. The hull surface is assumed to be hydrodynamically smooth (no roughness included) for both the model-scale and full-scale vessel. The size of the computational domain follows the ITTC recommendation("'Practical guidelines for ship CFD applications' 2014"). The distance from the inlet to the ship is twice the Length between perpendiculars (Lpp), and the outlet is located three times the Lpp away from the aft hull. Figure 1 shows the boundary conditions defined for the computation domain. The inlet and exterior boundaries are defined as velocity inlets, the outlet boundary as a pressure outlet, and and the hull is treated as a stationary no-slip wall. Drift angles were simulated by adjusting the flow direction at a constant Froude number of 0.165. The water density is 1024 kg/m³ with a Reynolds number (Rn) of 9.257×10^8 for the full-scale simulation, while the model scale uses a density of 999 kg/m³ and corresponding to a of 8.376×10^6. The domain discretisation is performed using the STAR-CCM+ mesh generator and consists of unstructured grids, including trimmed cells (hexahedrals) with local refinements at the aft part of the hull, as well as prism layers meshes along the hull surface. Figure 2 shows the grid, which features local refinement near the hull, comprising approximately 9.1 million cells at full scale and 6 million at model scales. The y^+ target is below 1, and the wall-resolved approach is used for both cases employing the k-ω SST turbulence model. Grid convergence studies were performed to assess numerical uncertainties in model-scale and full-scale. Beside the coarsest grid three finer grids are generated with a refinement ratio of $\sqrt{2}$,$\sqrt{3}$ and 2 respectively.

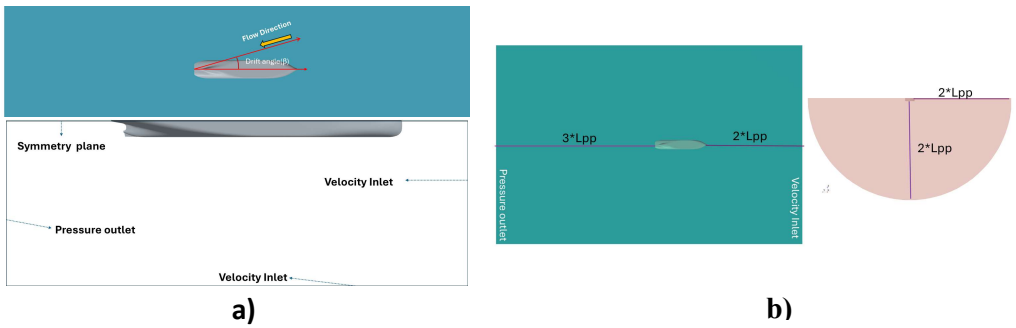

Fig. 1: a) Computational domain definition and boundary conditions b) Domain sizes

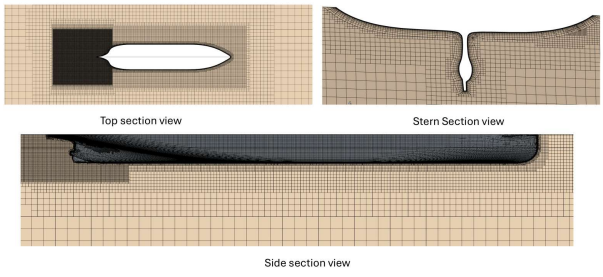

Fig. 2: Grid overview

To efficiently visualise nominal wake distributions for different drift angles without additional CFD simulations, POD-RBF methods provide an effective predictive method. POD-RBF is a data-driven reduced-order modelling approach that combines POD for high dimensionality reduction and RBF for

interpolation. First, POD extracts the optimal basis expansion from sampled CFD data at specified design points by representing the flow field as a truncated series of dominant modes (numerical eigenvectors), effectively capturing the most energetically significant flow features while achieving dimensionality reduction. Next, this POD expansion is coupled with radial basis function (RBF) training to create an interpolation model, enabling the prediction of field solutions at new, unsampled design parameter values. Together, these steps allow efficient and accurate reconstruction of the system's behaviour across a broader parameter space without requiring additional high-fidelity simulations. The details of this method are explained by (Huayamave et al., 2017). For the wake prediction in this study, the drift angles 1°, 3°, 6°, and 8° will be used to train the POD model, and the drift angles 0° and 9° will be used as references to verify the full-scale results.

3 Results and discussions

3.1 Numerical uncertainty analyses

The numerical uncertainty in the CFD simulation must be carefully considered. A numerical uncertainty defines an interval that should contain the truth or exact solution. In this study, the uncertainty is calculated to estimate the accuracy of the simulations based on the procedure developed by L. Eça and M. Hoekstra (Eça and Hoekstra, 2014). The grid refinement ratio and the simulation number cells are presented in Table 2. Figure 3-a presents, on the left, the model scale used to calculate the uncertainty U from the simulation. Figure 3-b shows the full-scale fit, with a numerical uncertainty of around 7.2% for the finest grid. The total resistance is plotted against the relative step size, with the fine mesh corresponding to a relative step size of 1. The numerical uncertainty of the finest grid in model scale is around 8.6% which is slightly larger than that of the full scale.

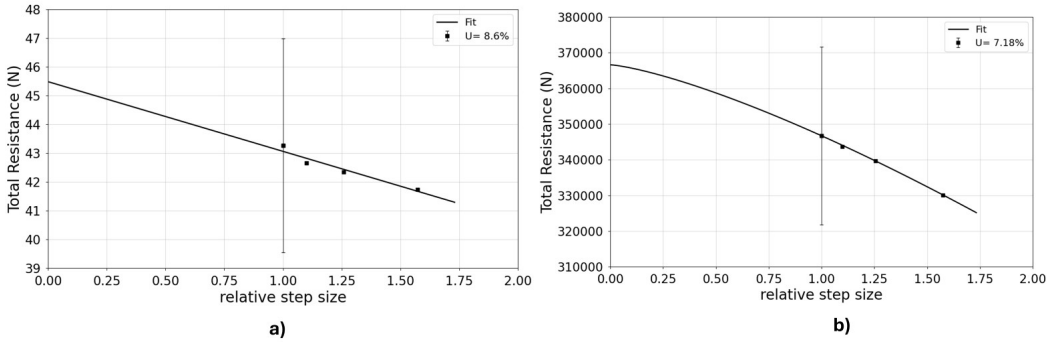

Fig. 3: The numerical uncertainty of the hull viscous resistance for a) model and b) full scale

Table 2: Number of cells for full scale and model scale simulation for the mesh study.

Refinement ratio	Number of cells for full scale simulation $\times 10^6$	Number of cells for model scale simulation $\times 10^6$
1	9.048093	2.402800
$\sqrt{2}$	24.720561	6.333127
$\sqrt{3}$	44.827439	11.396937
2	68.265738	17.028421

3.2 Resistance and side forces components analysis

With the double body RANS simulations, the resistance components can be estimated. However, the wave resistance is not calculated because of the absence of free-surface modelling in this approach. Pressure resistance coefficients show 20% to 96% reduction across the 0° to 9° drift angle range, with

model-scale results showing the minimum decrease (20%) and full-scale cases demonstrating almost complete elimination (96%) of pressure resistance at maximum drift angle, as shown in Fig. 4. However, the frictional resistance coefficient increases between 1.8 and 3.5% with the drift angle change. As a result, the total resistance coefficient remains nearly constant (within ±1%) for the model scale, while decreasing by up to 12% for the full-scale configuration. The observed reduction in pressure resistance primarily stems from decreased pressure magnitudes along the hull's bottom and stern regions at high drift angles, as shown in Fig. 5. This pressure drop occurs consistently at both full and model scales. The difference between full-scale and model-scale total resistance coefficients is due to scale effects, particularly differences in boundary layer development.

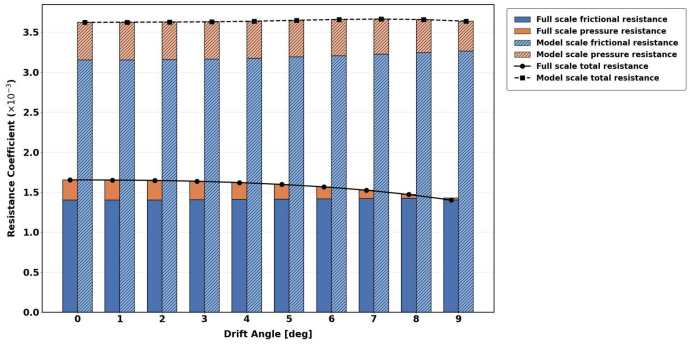

Fig. 4: Resistance component coefficients of the bare hull (forces in longitudinal direction)

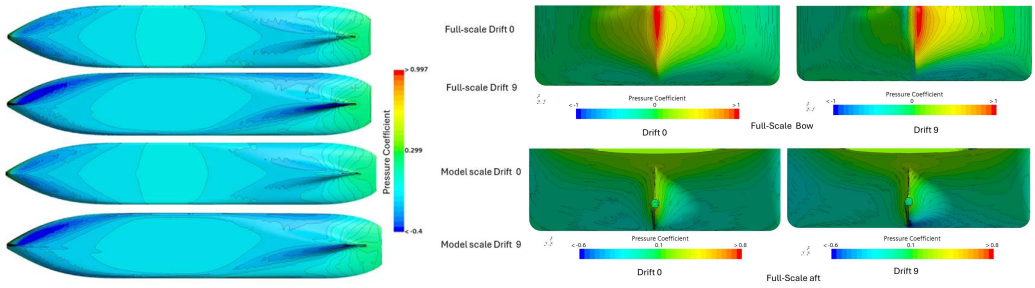

Fig. 5: Pressure distribution around the hull

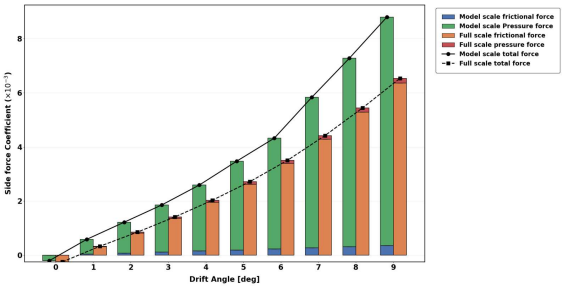

Fig. 6: Side force components coefficient variation at different drift angles

While resistance forces are conventionally computed in the X-direction (ship's longitudinal axis), the lateral forces (Y-direction) must also be evaluated, as they directly reflect the hull's side force variation with drift angle. This lateral force component becomes increasingly significant at higher drift angles due to asymmetric pressure distribution and possibly flow separation, as shown in Fig. 6. Both the frictional and pressure side forces increase. However, the pressure side force increases significantly,

almost 3 times the pressure resistance. The full-scale configuration shows a 43.70% average increase in pressure force per degree of drift angle, whereas the model-scale results exhibit a slightly higher increase rate of 50.75%.

3.3 Wake analysis

Accurate characterisation of flow behaviour at the propeller plane is essential for optimising propeller performance and avoiding cavitation risks. The nominal wake was extracted from the RANS simulations to assess flow characteristics. The nominal wake fields at the propeller plane are calculated by using equation 1.

$$w = 1 - Va/Vs, \qquad (1)$$

where, Vs is the ship speed and Va is the local flow velocity at the propeller plane. Figure 7 illustrates the nominal wake fields at the propeller plane. At 0° drift, the wake is concentrated near the center with uniform bottom-side distribution. At 9° drift, the wake disperses over a larger area with higher values, indicating expanded low-speed flow regions that may impact propeller performance. The model-scale wake exhibits more substantial flow discontinuity than the full-scale wake due to boundary layer effects. Figure 8 shows the mean wake at full and model scale for different drift angles. The mean wake increases between 1° and 3° degrees and starts decreasing up to a drift angle of 9°. Overall, the model-scale wake appears to decrease more significantly than the full-scale wake.

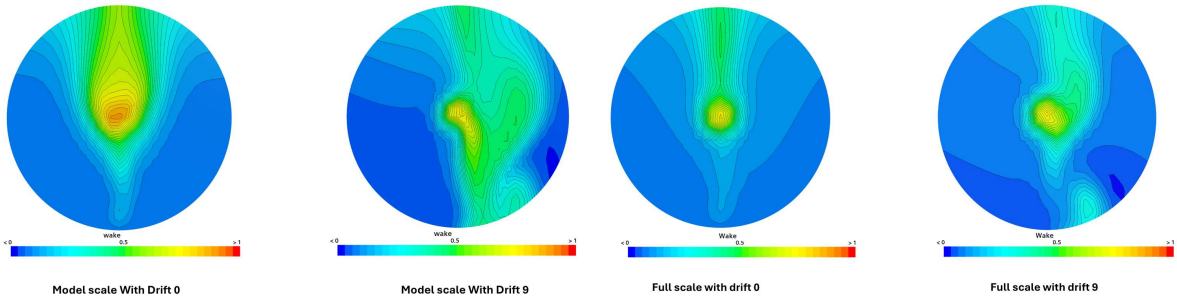

Fig. 7: Nominal wake field at the propeller plan at full and model scale

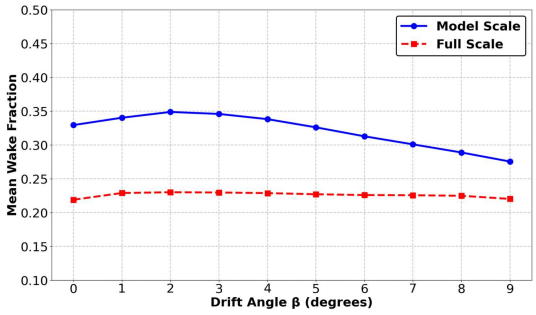

Fig. 8: Mean wake for full and model scale

3.4 POD-RBF prediction

The POD-RBF model enables fast prediction of the wake field in after training on CFD full-scale simulation data while maintaining good accuracy, as demonstrated in Fig.9 and Fig.10. The predictions show average errors of 7.9% for the 0° drift case in Fig. 9 and 5.4% for the 9° drift case in Fig. 10. The higher error at 0° drift likely results from insufficient training data. The CFD simulations took

approximately 16 core-hours for each drift angle, both for full scale and model-scale simulations. In contrast, the POD method can predict the wake flow in just a few seconds.

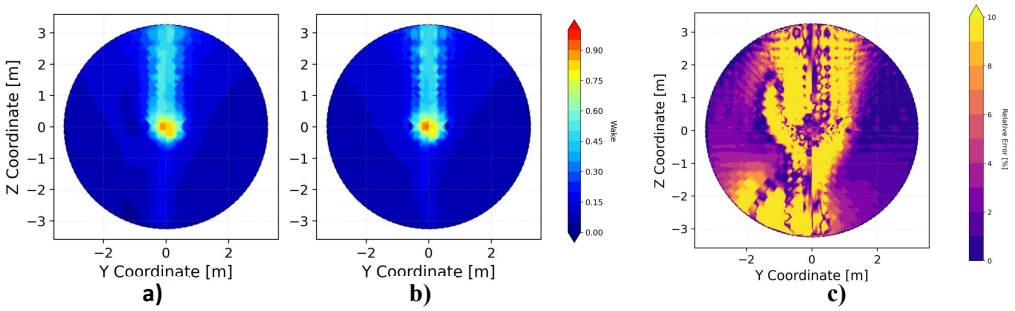

Fig. 9: Full-scale wake at drift angle 0° a) POD prediction, b) CFD reference result, c) Error between the POD deduction and CFD

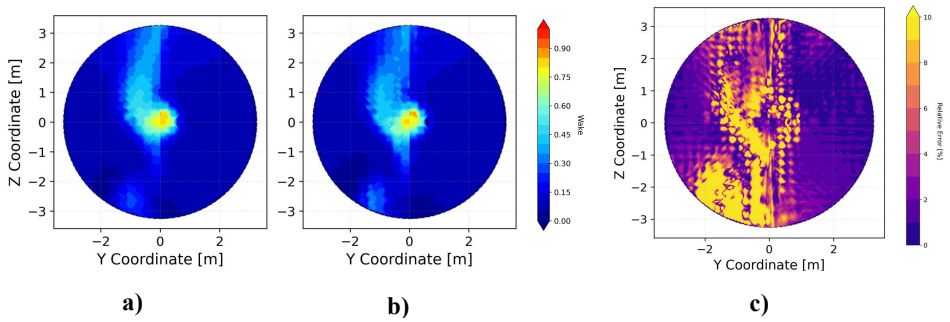

Fig. 10: Full-scale wake at drift angle 9° a) POD prediction, b) CFD reference result, c) Error between the POD deduction and CFD

4 Conclusion and Future Work

Both full- and model-scale analyses of drift angles reveal significant pressure resistance variations with drift angle, though total resistance remains relatively stable. Notably, side forces increase significantly, reaching triple the ship's resistance force at maximum drift. The POD-RBF method demonstrates good predictive capability for wake fields, maintaining low error relative to CFD results. Future work should incorporate free-surface effects to evaluate wave resistance and coupled drift angle impacts on both resistance and wake characteristics.

References

Ammar, N.R., and Seddiek, I.S., 2022. Wind assisted propulsion system onboard ships: case study Flettner rotors. Ships and Offshore Structures 17, 1616–1627. https://doi.org/10.1080/17445302.2021.1937797

Clayton, B.R., 1987. Wind-assisted ship propulsion. Physics in Technology 18, 53. https://doi.org/10.1088/0305-4624/18/2/301

Eça, L., Hoekstra, M., 2014. A procedure for the estimation of the numerical uncertainty of CFD calculations based on grid refinement studies. Journal of Computational Physics 262, 104–130. https://doi.org/10.1016/j.jcp.2014.01.006

Huayamave, V., Ceballos, A., Barriento, C., Seigneur, H., Barkaszi, S., Divo, E., Kassab, A., 2017. RBF-trained POD-accelerated CFD analysis of wind loads on PV systems. International Journal of Numerical Methods for Heat & Fluid Flow 27, 660–673. https://doi.org/10.1108/HFF-03-2016-0083

Ouchi, K., Uzawa, K., Kanai, A., Katori 2013"Wind Challenger" the Next Generation Hybrid Sailing Vessel.

Procedings, I. T. T. C. "Practical Guidelines for Ship CFD Applications ITTC–Recommended Procedures and Guidelines." International Towing Tank Conference section. Vol. 7. 2014.